An insight on the design of mercapto functionalized swelling brittle micas

Francisco J. Osuna,[1] Esperanza Pavón,[1] María D. Alba[1,*]

[1] Instituto Ciencia de los Materiales de Sevilla (CSIC-US). Avda. Américo Vespucio, 49. 41092 Sevilla, Spain

Abstract.

Surface modification of natural clay minerals with reagents containing metal chelating groups has great environmental value. The functionalization by adsorption or grafting guarantees a durable immobilization of the reactive organic groups, preventing their leaching when they are used in liquid media. The aim of this research was the designed mercapto functionalization of swelling brittle micas, Na-M*n*, thorough both chemical and physical mechanisms. Na-M*n* were functionalized with 2-mercaptoethylammonium (MEA), 2,3-dimercapto-1-propanol (BAL) and (3-mercaptopropyl)trimethoxysilane (MPTMS). The thiol concentration on swelling brittle micas is higher than the observed value for others adsorbents. The cation exchange reaction with MEA and one-step grafting with MPTMS in acid medium are the most efficient mercapto functionalization mechanism.

Keywords. Designed materials; grafting; functionalized surface; thiol groups

* Corresponding author: alba@icmse.csic.es

1. Introduction

Industrial activities increases the load of potentially toxic compounds in the environment and, thus, there is a growing demand for development of materials and methods to remove toxic compounds from aqueous solutions. Reverse osmosis, ion exchange, coagulation, flocculation, chemical oxidation, biological processes and adsorption are some of the process used for micro pollutants removal. However, some of them cannot be applied due to high cost, use of chemical reagents and the formation of unknown oxidation intermediate compounds [1]. In this context, many studies have reported the use of the adsorption method as an efficient and low cost procedure in the removal of several micro pollutants, silicate-based materials being a very attractive option [2-4].

Clays minerals such as smectites have been widely used as sorbent of heavy metals in spite of their limited adsorption capacity, relatively small metal binding constants and low selectivity to the type of metals [5]. Surface modification of natural clay minerals with reagents containing metal chelating groups has been explored in an effort to enhance both the selectivity and the heavy metal binding constants [6, 7]. To overcome those problems, the surface of clay minerals can be modified throughout the incorporation of organic moieties into the interlayer space, both intercalated or grafted [8, 9]. The intercalation is a physical adsorption but grafting is a process that links the inorganic and organic components via strong bonds such as covalent or ionic-covalent to obtain functionalized clays [10]. This approach enables a durable immobilization of the reactive organic groups, preventing their leaching when they are used in liquid media.

Among all the surface modifications, the functionalization of silicates with thiol groups has been extensively studied for heavy metal cation immobilization [11] because the thiol groups exhibit a high binding selectivity toward the target metal cations [12] and

the metal adsorption is being directly associated with the amount of SH available in the absorbent [13]. Many efforts have been dedicated to the grafting of silicate-based materials with organic functional groups to provide more stable hybrid compounds [14-17]. Organic functional groups such as amine, thiol, carboxylate, shift base are considered as promising molecules to favor the interaction with heavy metals, dyes, and some phenols and pharmaceutical residues [2, 18, 19].

In this environmental context, novel materials are increasingly being sought-after to remove pollutants from water [20]. A new family of synthetic fluorophlogopite, Na-M*n*, has demonstrated to be attractive adsorbents for their unique combination of high layer charge, *n,* ranging between 2 and 4, swelling capacity and cation exchange properties, up to 4694.84 meq/kg [21-24]. Moreover, their chemical and physical properties can be easily tuned by an appropriated synthesis design. Their layer charge derives from the tetrahedral substitutions and hence, these high charged micas behave as a hard base [25]. Consequently, the as-made micas are better adsorbents of hard or intermediate acids such as Cu^{2+} or Pb^{2+} than soft acid such as Cd^{2+} or Hg^{2+} [26]. The enhancement of their adsorption capacity and affinity by soft acid cations can be achieved by functionalization with thiol groups [27-29]. Up to our knowledge, there is not any report on swelling high charged micas functionalized with thiol groups in spite of their demonstrated capacity of harmful cations removals [21, 30-33].

Therefore, our aim was the preparation and characterization of mercapto functionalized swelling brittle micas. Both physical (sorption) and chemical (grafting) functionalizations have been explored to enhance the amount of available SH groups, which could provide more adsorption sites for cationic pollutants. With this goal, parameters such as pH, time, thiol source and concentration have been explored.

2. Materials and methods

2.1. Materials

The synthesis method employed was the described by Alba et al. [21]. Powder mixtures with molar composition: (8 - *n*) SiO_2, (*n*/2) Al_2O_3, 6 MgF_2, and (2*n*) NaCl (*n* is the layer charge per unit cell, *n* = 2 and 4) were used. The starting materials were SiO_2, $Al(OH)_3$, MgF_2 and NaCl and their chemical sources and purities are listed in Table S1. All reagents were mixed and ground in an agate mortar and, then, heated in air up to 900 °C for 15 h, in a Pt crucible. Finally, the solids were washed with deionized water and dried at room temperature. The as-synthesized samples were named as Na-M*n* (*n*= 2 and 4) and with a nominal cation exchange capacity, CEC, of 2475.25 and 4694.84 meq/kg, respectively.

2.2. Thiol functionalization

2.2.a. *Intercalation*

The intercalation of 2-mercaptoethylammonium (MEA) and 2,3-dimercapto-1-propanol (BAL) into the mica structure was carried out following the procedures described by Tran et al. [34, 35]. The source and purity of all the chemicals have been included in Table S1.

3.0 g of Na-M*n* were dispersed in 60 ml distilled water under 10 min ultrasound shaking for MEA functionalization while 500 mg of Na-M*n* were dispersed in 10 ml of ethanol under 10 min ultrasound for BAL functionalization. Second, a certain amount of MEA and BAL, equivalent to three times their cation exchange capacities, were added to the solution. The pH values of the mixtures were adjusted up to 1 with HCl. The reaction conditions (time, medium and temperature) are displayed in Table 1. After the reaction

was completed, the functionalized samples were collected by centrifuging (MEA-M*n*) or filtering (BAL-M*n*), washed as stated in Table 1, dried at RT and ground manually.

2.2.b Grafting

1-step and 2-steps reactions are explored in order to stablish the best experimental conditions to graft mercapto functional groups on swelling high charge micas. The source and purity of all chemicals have been included in Table S1.

1-step grafting. 1-step grafting was explored under three different pH (acid, basic and neutral). 500 mg of Na-M*n* were dispersed in 10 ml of ethanol (SH-Mn-1-Ac), 25 ml of methanol (SH-Mn-1-Ba) and dry toluene (SNa-Mn-1, 1-t and 1-c). Later, 3-mercaptopropyl trimethoxysilane (MPTMS) was added to the suspension (see Table 1 for amounts). The pH values of the acid and basic mixture were adjusted to 1 by 1 M HCl (SH-Mn-1-Ac) and with 100 ml of 0.05 M NaOH, final pH value of 13, (SH-Mn-1-Ba). The resulted mixtures were shaken in an orbital shaker at 125 rpm for 24 h or 72 h (Table 1). When the reactions were completed, the functionalized samples were collected by filtering and washed (see Table 1), dried at RT or at 120ºC under vacuum for 2 h and ground manually.

The samples were named as S*x*-M*n*-1-*y*, where *x* indicates the nature of the interlayer cation of the starting mica (Na^+ or H_3O^+); *n* is the mica charge layer (2 or 4); and; *y* is the reaction medium (Ac=acid, Ba=basic, and, null is neutral).

2-step grafting. Within this approach, samples are first acid treated to enhance the active adsorption sites to perform the chemical incorporation of MPTMS molecules.

Acid-attacked samples were prepared as follow: 1 g of Na-M*n* was dispersed in a solution of 0.15 M HCl and shaken overnight. Two different acid/mica ratio were explored to analyse the effect on the acidification of the silicates (7.5 and 24.5 mmol

HCl/g mica for H-Mn-2-A and H-Mn-2-B, respectively). The pH of the mixtures were adjusted by water (18 MΩ/cm^3) up to neutral pH. The solids were collected by filtering, dried at RT and ground manually.

In the second step, a procedure similar to the one described by Ferreria Guimaraes et al. [27] was applied. 500 mg of pre-acid silicates (H-Mn-2-A and H-Mn-2-B) were dispersed in a solution of 0.2 M 3-mercaptopropyl trimethoxysilane (MPTMS) in dried toluene at two different MPTMS:mica ratios (Table 1). The resulted mixtures were shaken in an orbital shaker at 125 rpm under Ar atmosphere during 24 h or 72 h. When the reaction was completed, the functionalized samples were collected by filtering and washed with toluene (three times) followed by one ethanol washing. The solids were dried at 120 ºC in vacuum for 2 h and ground manually.

The samples were named as SH-M*n*-2-*z*, where *n* is the mica charge layer (2 or 4); and; *z* indicates the experimental variables: A or B indicates the pre-acid treatment condition; t is the variable time; and; c is the variable MPTMS concentration. All the preparation details are summarized in Table 1 and Fig. 1.

2.3. Characterization

ICP-AES (Inductively Coupled Plasma-Atomic Emission Spectrometry) was used to analyse the sulphur content on the functionalized samples. Measurements were carried out at microanalysis laboratory (CITIUS, University of Seville, Spain) using a HORIBA JOBIN YVON-ULTIMA 2 equipment.

Powder X-ray diffraction (XRD) was carried out to check the phase purity, to determine the basal spacing of the micas, and to monitor crystallinity. XRD patterns were obtained at the X-ray laboratory (CITIUS, University of Seville, Spain) on a Bruker D8 Advance instrument equipped with a Cu K_α radiation source operating at 40 kV and 40

mA. Diffractograms were obtained in the 2θ range of 3–70° with a step size of 0.015° and a step time of 0.1 s.

FTIR spectra were recorded in the range 4000–400 cm^{-1} in the Spectroscopy Service of the ICMS (CSIC-US, Seville, Spain), as KBr pellets dried at 120 ºC, using JASCO FT/IR-6200 IRT-5000 instrument.

MAS-NMR experiments were performed on a Bruker AVANCE WB400 spectrometer equipped with a multinuclear probe, in the Nuclear Magnetic Resonance Service of University of Córdoba (Córdoba, Spain). Powdered samples were packed in 3.2 mm zirconia rotors and spun at 10 kHz. ^{13}C MAS NMR spectra were recorded at 104.26 MHz. The single pulse with proton decoupling (SP) spectra were recorded with a pulse width of 2.5 μs (π/2 pulse length = 7.5 μs) and a delay time of 2 s and the cross polarization ^{1}H-^{13}C (CP) spectra were recorded with a π/2 pulse length of 2.3 μs, contact time of 2 ms and a delay time of 4 s. ^{23}Na MAS-NMR spectra were recorded at 105.84 MHz with a pulse of 0.75 μs (π/12) and a delay time of 0.1 s. ^{29}Si MAS-NMR spectra were acquired at a frequency of 79.49 MHz, pulse width of 2.7 μs (π/6) each 3 s. ^{27}Al MAS-NMR spectra were recorded at 104.26 MHz with a pulse of 0.38 μs (π/20) and a delay time of 0.5 s. The chemical shift values were reported in ppm from tetramethylsilane for ^{13}C and ^{29}Si, and from a 0.1 M $AlCl_3$ and NaCl solution for ^{27}Al and ^{23}Na, respectively.

The binding energy of the sorbents was analysed using X-ray photoelectron spectroscopy at the XPS Service (CITIUS, University of Seville, Spain). The XPS spectrometer "Leybold-Hereus" mod. LHS-10/20 is equipped with a twin anode (Mg and Al) monochromatized X-ray source and a multichannel EA200 analyser. All scans given in this work were obtained with the Al source and binding energies were reference to C (1s) signal at 284.8 eV.

3. Results and discussion

The amount of thiol incorporated into the micas has been obtained by ICP (Fig.2) and it depends on the experimental conditions as well as on the mica layer charge. The thiol concentration ranges between 9.4 and 3409.4 mmol/kg, which is of the same order than other silicate adsorbents (Table S2), noticeable the highest thiol concentration is higher than the maximum observed in the literature (Swy-1, 3200 mmol/kg) [7, 11, 36, 37].

3.1 Intercalation

MEA-M*n* contains a significantly larger amount of SH groups than BAL-M*n*, despite the later contains double amount of thiol groups per molecule (Fig. 2). This may indicate different adsorption mechanisms, whereas MEA, an organic cation, can be exchanged with the interlayer Na^+, neutral BAL can be only adsorbed on the surface. The two different mechanisms could explain that the amount of thiol group is not influenced by the layer charge in BAL-M*n* while it increases with the layer charge in MEA-M*n*.

X-ray diffractograms of the Na-M*n*, *n*=2 and 4 (Fig. 3) show patterns that correspond to that previously reported for swelling high-charged micas [38] with a unique *001* reflection corresponding to a basal space of 1.22 nm due to hydrated Na^+ in the interlayer space [39].

After functionalization with MEA (Fig. 3), the d_{001} shifts to ca. 1.65 nm; an additional basal spacing is observed at 1.30 nm in both micas while other two reflections, corresponding to 1.57 nm and 1.46 nm, in MEA-M2 are detected. This may denote a less ordered configuration of the organic chain in the interlayer space of the mica with the lowest layer charge. The functionalization with BAL (Fig. 3) does not significantly

change mica basal spacing, corroborating that it has not been intercalated in the interlayer space as previously reported for montmorillonite and vermiculite [35].

The IR/FT spectra of Na-M*n* (Fig. 4) show bands at 3525 cm^{-1} due to the H-O-H stretching vibration of adsorbed water molecules in the tetrahedral sheets. [40] The bands at ca. 1000 cm^{-1} correspond to the Si-O-Si and Si–O–Al groups of the silicate layers, which shift to higher frequency in Na-M2 (979 and 1009 cm^{-1} vs 965 cm^{-1} in Na-M4) [41].

In the spectrum of MEA-M*n* (Fig. 4), the band at ca. 3500 cm^{-1} is due to residual H-O-H stretching vibration. The broad band at ca. 3000 cm^{-1} and those marked with asterisk at 1459 cm^{-1}, 1506 cm^{-1}, 3252 cm^{-1} are identified as the aliphatic C-H stretching and deformation vibrations or N-H bending vibrations of MEA [36, 42] suggesting that MEA has been successfully introduced into the micas. No change in the vibration band of Si-O-Si and Si–O–Al groups of the silicate layers, ca. 1000 cm^{-1}, is observed. In the case of BAL-M*n* (Fig. 4), new small peaks are observed to emerge at 1427 cm^{-1} from aliphatic C-H deformation of BAL [36, 43] and also a broad band at ca. 3428 cm^{-1} due to O-H stretching vibration [44] is observed, both features imply the successful loading of BAL molecules on micas. However, the expected S-H stretching band of the thiol functionality (at about 2575 cm^{-1}) cannot be observed, which may be attributed to the aggregation or weakness of mercapto groups within the pure compounds and the hydrogen binding effects [45].

All the results indicate that MEA loading into mica is favoured, probably due to its positive electric charge.

3.2. Grafting

The thiol concentration in 1-step MPTMS grafting (Fig. 2) depends on the pH, being the use of an acid medium the most effective procedure for the mercapto functionalization, followed by the basic medium and last, the neutral one. When using the 2-steps approach in the functionalization, the results are better than those obtained for the neutral medium and more thiol groups are incorporated into the structure, however their value are not close to 1-step acid or basic medium.

When comparing the influence of the mica layer charge, Mica-2 samples exhibit higher thiol adsorption capacity in acid medium (1-step or 2-step). This is due to the higher chemical stability at acid pH that micas with lower layer charge exhibit [46, 47].

1-step grafting does not produce any change in the interlayer space of the mica in the neutral or basic medium (Fig. 5) regardless the layer charge. However, when acid medium is employed a shift of the *001* reflection to higher basal space is observed (around 1.4 nm) for the mica with the lower layer charge (SH-M2-1-Ac). In SH-M4-1-Ac, a small shoulder in the *001* reflection is also observed.

The acid pre-treatment in the 2-step grafting affects the *001* reflection that shifts to higher basal space (around 1.4 nm) probably due to Mg^{2+} and/or Al^{3+} leaching to the interlayer space (Fig. S1, H-Mn-2-A and H-Mn-2-B). Moreover, the XRD of acid activated samples show an increase of the background in the interval 19 and 30º 2Θ due to the dissolution of mica and deposition of amorphous material (Fig. S1). Other researchers reported similar increase in the background after acid treatment of clay minerals [48-50]. The highest acid medium, with 24.5 mmol HCl/g mica in Na-M4 (H-M4-2-B), provokes the disappearance of the *001* reflection, indicating the breaking of mica layer structure.

In general, no alteration in the XRD of micas modified with MPTMS (Fig. 5) in comparison with their starting acid samples is observed as previously reported in the

literature.[51] Reduction of basal spacing in SH-M4-2-A, SH-M4-2-t and SH-M4-2-c may be explained by the elimination of water molecules from the interlayer during the grafting [51].

IR-FT spectra of the 1-step grafting samples in acid and basic media (SH-Mn-1-Ac and SH-Mn-1-Ba, Fig. 6) show the bands attributed to the -SH groups and stretching of -CH_2 of MTPMS, marked with asterisk. However, these lines are not observed in the 1-step neutral samples regardless the reaction time or the MPTMS concentration used (SNa-Mn-1, SNa-Mn-1-t, SNa-Mn-1-c), due to the features overlapping.

The 1-step grafting does not produce any alteration in the stretching bands of Si-O-M (M=Si or Al) regarding the starting samples. However, they shift to higher frequency because of the pre-acid treatment in the 2-step grafting (Fig. 6 and Fig. S2), confirming the leaching of tetrahedral aluminium that could be responsible of the higher basal space observed by XRD. Similar results have been reported in others clay minerals [52]. In the case of Na-M4, when the acid treatment is severe (H-M4-2-B), those bands disappear as an indicative of the framework breakdown as previously observed by XRD.

3.3. *Short range structural order analysis*

The interlayer and framework short-range structural order of the samples with the most efficient thiol functionalization (MEA-M*n* and SH-M*n*-1-Ac) has been analysed by MAS NMR and XPS spectroscopies.

The ^{29}Si MAS NMR spectra of the Na-M*n* (Fig. 7) can be described in terms of a set of signal between -70 and -90 ppm, compatible with the existence of several single Q^3(mAl) environments as expected for 2:1 layered aluminosilicates [21]. Two others signals, centered at ca. -61.7 ppm and at ca. -85 ppm, appear in the Na-M2 previously assigned to Q^0 silicon environments from forsterite [53] and sodalite [21, 39]. In Na-M4,

a fifth peak is observed at ca. -75 ppm that points to a violation of Lowenstein's rule [54, 55].

The physical incorporation of thiol groups in the mica structure provokes a distortion in pseudohexagonal hole of the tetrahedral layer, as it can be observed in the ^{29}Si MAS NMR signals of MEA-M*n* (Fig. 7) that are shifted by 2.5 ppm towards lower frequencies with respect to the original sodium mica. We have previously observed a similar shift of the ^{29}Si frequencies in micas exchanged with different interlayer organic cations, due to the location of the polar part of the surfactant close to the basal oxygen plane. A tilt of the organic molecule facilitates the incorporation of the NH_3^+ moiety into the pseudohexagonal hole [56, 57], as demonstrated by the shift of the ^{29}Si NMR signals.

Nevertheless, the exchange process between Na-M*n* and MEA does not alter the Si and Al distribution, as shown in the ^{29}Si spectra where all the relative intensities of the Q^3(mAl) peaks are similar.

Thiol chemical incorporation, on the other hand, does not affect the position of the Q^3(mAl) signals in the ^{29}Si spectra, that remains unaltered with respect to the original Na-M*n* but it does change the Q^3(mAl) relative intensities, mainly a reduction of Q^3(3Al) signal is observed. Moreover, two new signals at ca. -57 and -67 ppm appear. Mercier et al. [7] attributed them to isolated mercaptopropyl groups (T1) and fully cross-lined mercaptopropyl groups (T2), respectively. This demonstrates that the mercaptopropyl groups have been successfully grafted into the M-OH (M=Si and/or Al) of the mica.

The alteration of the framework cation distribution due to the physical or chemical mercapto incorporation into the mica structure can be completed with ^{27}Al MAS NMR (Fig. S3). MEA-M*n* spectra are similar from those of starting samples because the exchange reaction of interlayer sodium by MEA does not affect the framework cation distribution. Hence, an asymmetric band at ca. 67 ppm corresponding to aluminum in

tetrahedral coordination together with a peak at ca. 0 ppm, arising from octahedral coordination, only observed in *n*=4 samples, can be distinguished in the spectra [58-60].

However, the grafting with MPTMS in acid media (SH-M*n*-1-Ac) provokes an increment of the signal from the octahedral coordinated aluminium, meaning that an aluminium leaching from the tetrahedral layer to the interlayer space is occurring in the MPTMS chemical incorporation. This leaching would explain, as well, the decrease in the Q^3(3Al) relative intensities shown above.

The ^{23}Na MAS-NMR spectra of samples Na-M*n* (Fig. 8) are characterized by two signals: i) a main one between 0 and -25 ppm due to hydrated interlayer sodium [61]; and; ii) a broad one at ca. 27 ppm from non-exchangeable sodium [62]. After MEA functionalization, the signal from the hydrated sodium almost disappear, indicating that the initial interlayer Na^+ in the inorganic mica has effectively been replaced by the organic chain, acting the latter as interlayer cation. However, in thiol grafting, the interlayer hydrated Na^+ signal does not completely disappear, although it considerable decreases. This may be due to the exchange of interlayer Na^+ by framework Al^{3+} or Mg^{2+} leached because of the acid medium used in the reaction, as previously observed by ^{27}Al MAS-NMR spectroscopy (Fig. S3)

The state and configuration of the organic molecules can be analyzed thorough ^{13}C MAS NMR (Fig. 9). The ^{13}C MAS NMR spectrum of the MEA-M2 (Fig. 9) is characterized by four signals that can be assigned to two different cations: HS-CH_2-CH_2-NH_3^+ (signals marked with square and with slash pattern, 40 and 23 ppm respectively) and $^+H_2$S-CH_2-CH_2-NH_3^+ (signals marked with asterisk and in grey, 43 and 33 ppm respectively) [63]. In MEA-M4, two other signals are observed, at ca. 37 and 30 ppm, due to the multiplication of the carbon chain environments as a consequence of the remnant sodium in the interlayer space (only 72% of its CEC was satisfied by MEA, Fig. 2) [29].

The presence of the -CH_2-SH_2^+ group at natural pH (6.27) is in agreement with the less negative Zeta potential observed at acidic pH, as seen by Osuna et al [64] due to the protonation of the thiol group. In addition, the relative intensity of the ^{13}C MAS NMR signal corresponding to the -CH_2-SH_2^+ group is more intense in MEA-M4 than in the MEA-M2, which justifies that no changes in the Zeta potential values of the MEA-M2 at natural pH (5.80) were observed [64].

The ^{13}C MAS NMR spectra of SH-M*n*-1-Ac (Fig. 9) show all the carbons from the organic chain. The peak at ca. 13 ppm is due to de C3 of the mercaptopropyl chain, the peak at ca. 29 ppm corresponds to the C1 and C2 of mercaptopropyl chain, and, the peaks at ca. 44 ppm and ca. 55 ppm are attributed to the C4 of the metoxy group, in molecules with SH and SH_2^+ thiol group, respectively [63, 65]. This last is more evident in SH-M2-1-Ac, that the hydrolysis of the MPTMS is not complete. Two additional signals are observed at ca. 18 ppm and ca. 24 ppm that correspond to C2 and C3 of fully hydrolysed MPTMS [63].

Comparison of the ^{13}C SP and CP MAS NMR spectra of SH-M*n*-A (Fig. 9) shows changes in the peak intensities that demonstrates that MPTMS is present in different states: one mobile in the interlayer space and other rigid in a confined space [29].

Further evidence about the successful grafting of the thiol group into the structure of mica was obtained by XPS. The S 2p core-level spectra (Fig. 10) show bending energy of 163.1 eV for MEA-M*n* and 163.8 eV for SH-M*n*-1-Ac, which are attributed to the sulphur element in –SH group [35]. The binding energy value of SH-M*n*-1-Ac is typical of S 2p signal of the silica-bound (3-mercaptopropyl)trimethoxysiloxane [66], which could be due to the chemical graphitization of the mica surface with thiol. However, the sulphur binding energy shifts to a less positive value, in MEA-M*n*, due to more-electronegative S atoms in the surface [67].

4. Conclusions

The thiol concentration on swelling brittle micas is higher than those observed for others clays. For the physical functionalization, the amount of thiol groups is considerable higher for MEA than BAL functionalization, in spite of BAL contains double thiol group per molecule than MEA. Thus, the cation exchange mechanism is more efficient for functionalization than sorption of polar molecules.

The grafting with MPTMS is more efficient when is performed in one-step in an acid medium. In this case, an incomplete polycondensation of silicic species occurs and the amount of fully cross-linked mercaptopropyl groups increases with the layer charge.

Therefore, potential effective metal adsorbents are provided from thiol grafting of the design micas with higher thiol content than those reported in the literature.

Acknowledgements

The authors would like to thank the Junta de Andalucía (Spain) and FEDER (Proyecto de Excelencia de la Junta de Andalucía, project P12-FQM-567), to the Spanish State Program R+D+I oriented societal challenges and FEDER (Project MAT2015-63929-R) for financial support. F.J. Osuna thanks his grant to the training researcher program associated to the excellence project of Junta de Andalucía (P12-FQM-567).

Appendix A. Supplementary data

Supplementary data to this article can be found online

Table 1.

Functionalization parameters of Na-M*n* (*n*= 2 or 4, layer charge); w: water; e: ethanol; t: toluene; m: methanol

		Sample name	Pre-step	Functionalization				
			mmol HCl/ g mica	Reaction medium	mmol mercpato molecule /g mica	t(h)	wash	dry
sorption		MEA-M2	--	w, HCl 0.1 M, 30ºC	7.4	24	w	air, RT
		MEA-M4	--	w, HCl 0.1 M, 30ºC	14.1	24	w	air, RT
		BAL-M2	--	e, HCl 1M, 80ºC	7.4	20	e, w	air, RT
		BAL-M4	--	e, HCl 1M, 80ºC	14.1	20	e, w	air, RT
grafting	2 steps	SH-Mn-2-A	7.5	t	10	24	t, e	vacuum, 120 ºC
		SH-Mn-2-B	24.5	t	10	24	t, e	vacuum, 120 ºC
		SH-Mn-2-t	7.5	t	10	72	t, e	vacuum, 120 ºC
		SH-Mn-2-c	7.5	t	25	24	t, e	vacuum, 120 ºC
	1 step	SH-Mn-1-Ac	--	e, HCl 1 M	7.3	24	w	air, RT
		SH-Mn-1-Ba	--	m, NaOH 0.05M	10	24	w, e	air, RT
		SNa-Mn-1	--	t	10	24	t, e	vacuum, 120 ºC
		SNa-Mn-1-t	--	t	10	72	t, e	vacuum, 120 ºC
		SNa-Mn-1-c	--	t	25	24	t, e	vacuum, 120 ºC

FIGURE CAPTIONS

Fig. 1. Schematic representation of the functionalization.

Fig. 2. Amount of sulphur per kg of mica

Fig. 3. XRD of the Na-M*n* functionalized by exchange reaction.

Fig. 4. IR/FT spectra at 120 ºC of the Na-M*n* functionalized by exchange reaction.

Fig. 5. XRD of the Na-M*n* after grafting.

Fig. 6. IR/FT spectra at 120 ºC of the Na-M*n* after grafting.

Fig. 7. Schematic representation of isolated (T1) and fully cross-linked mercaptopropylsilane groups and ^{29}Si MAS NMR spectra of the Na-M*n*, MEA-M*n* and SH-M*n*-1-Ac: a) *n*=2 and b) *n*=4.

Fig. 8. ^{23}Na MAS NMR spectra of the Na-M*n*, MEA-M*n* and SH-M*n*-1-Ac: a) *n*=2 and b) *n*=4.

Fig. 9. ^{13}C MAS NMR spectra of the MEA-M*n* and SH-M*n*-1-Ac (black line= ^{13}C (SP) MAS NMR spectra, and, red line=^{1}H-^{13}C (CP)MAS NMR spectra

Fig. 10. XPS spectra of the MEA-M*n* and SH-M*n*-1-Ac.

Fig. 1

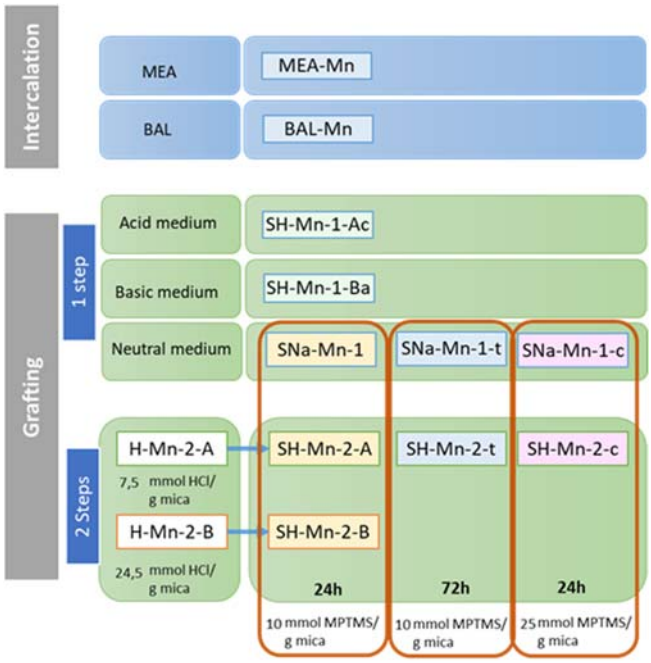
Intercalation
MEA
MEA-Mn
BAL
BAL-Mn
Grafting
1 step
Acid medium
SH-Mn-1-Ac
Basic medium
SH-Mn-1-Ba
Neutral medium
SNa-Mn-1
SNa-Mn-1-t
SNa-Mn-1-c
2 Steps
H-Mn-2-A
7,5 mmol HCl/ g mica
SH-Mn-2-A
SH-Mn-2-t
SH-Mn-2-c
H-Mn-2-B
24,5 mmol HCl/ g mica
SH-Mn-2-B
24h
72h
24h
10 mmol MPTMS/ g mica
10 mmol MPTMS/ g mica
25 mmol MPTMS/ g mica

Fig. 2

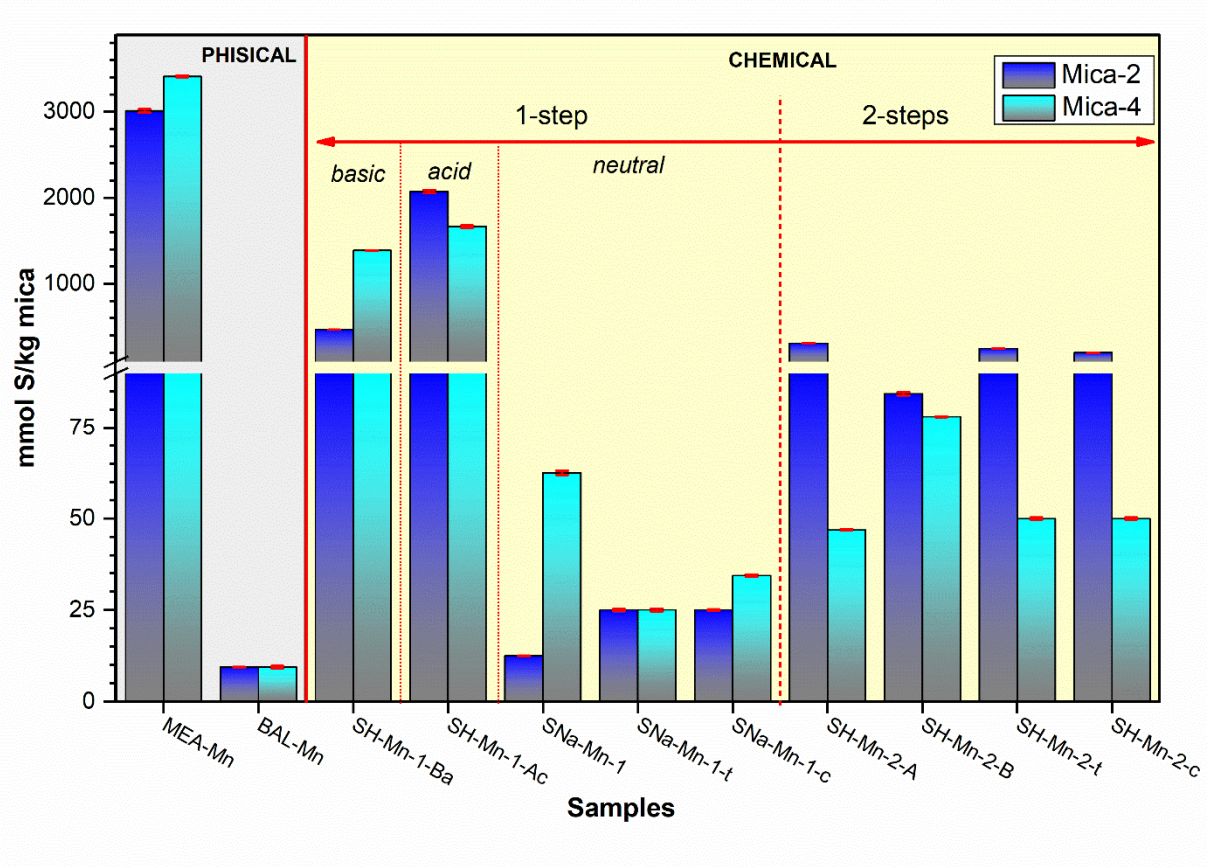
PHISICAL
CHEMICAL
Mica-2
Mica-4
1-step
2-steps
basic
acid
neutral
mmol S/kg mica
3000
2000
1000
75
50
25
0
MEA-Mn
BAL-Mn
SH-Mn-1-Ba
SH-Mn-1-Ac
SNa-Mn-1
SNa-Mn-1-t
SNa-Mn-1-c
SH-Mn-2-A
SH-Mn-2-B
SH-Mn-2-t
SH-Mn-2-c
Samples

Fig. 3

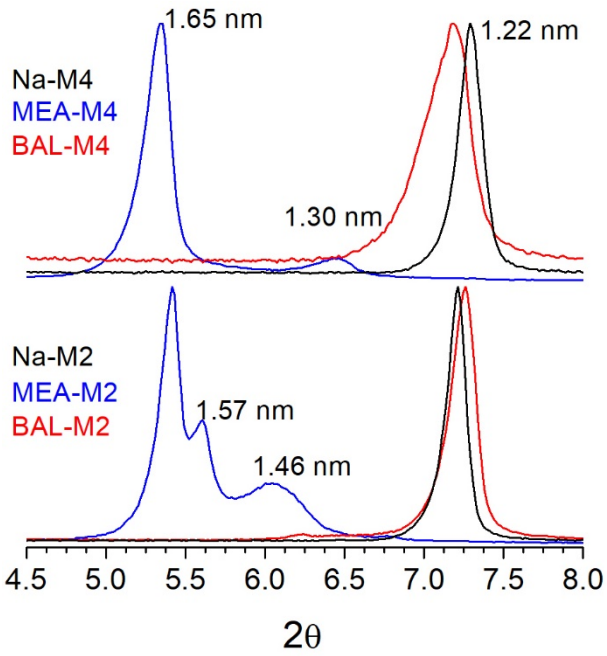
1.65 nm
1.22 nm
Na-M4
MEA-M4
BAL-M4
1.30 nm
Na-M2
MEA-M2
BAL-M2
1.57 nm
1.46 nm
4.5
5.0
5.5
6.0
6.5
7.0
7.5
8.0
2θ

Fig. 4

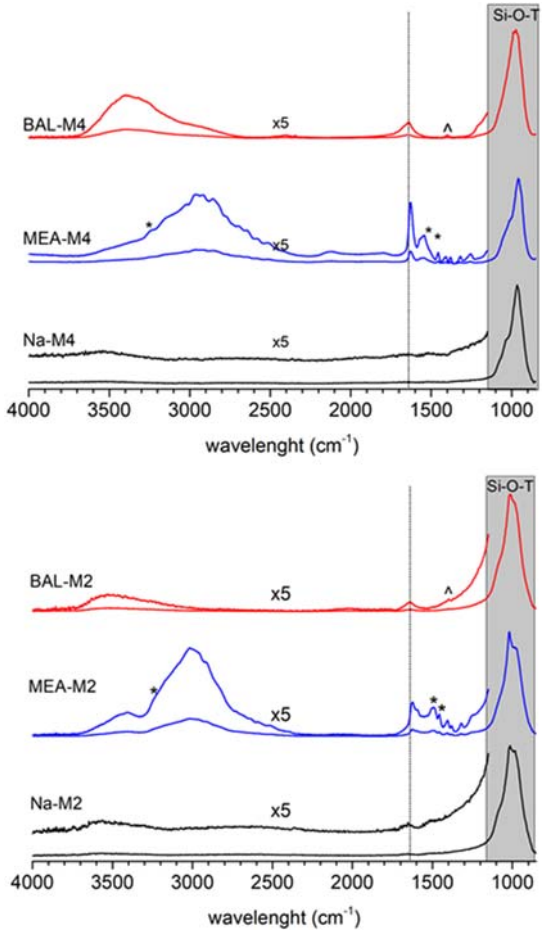
Si-O-T
BAL-M4
x5
^
MEA-M4
x5
*
* *
Na-M4
x5
4000
3500
3000
2500
2000
1500
1000
wavelenght (cm-1)
Si-O-T
BAL-M2
x5
^
MEA-M2
x5
*
* *
Na-M2
x5
4000
3500
3000
2500
2000
1500
1000
wavelenght (cm-1)

Fig. 5

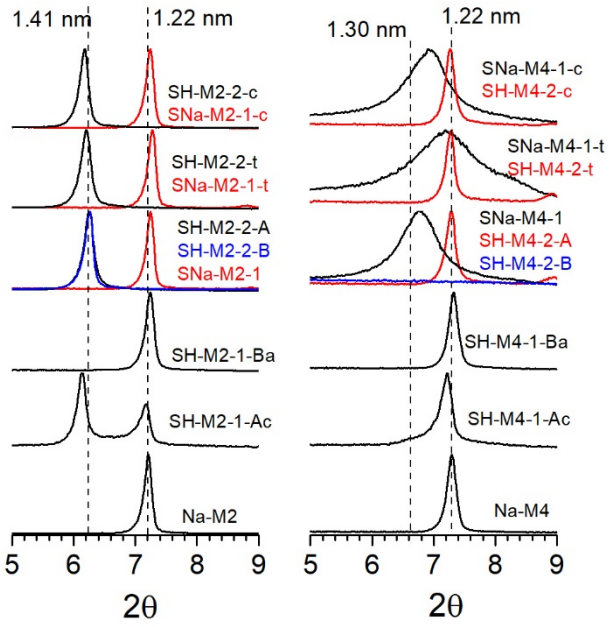
1.41 nm
1.22 nm
SH-M2-2-c
SNa-M2-1-c
SH-M2-2-t
SNa-M2-1-t
SH-M2-2-A
SH-M2-2-B
SNa-M2-1
SH-M2-1-Ba
SH-M2-1-Ac
Na-M2
5 6 7 8 9
2θ
1.30 nm
1.22 nm
SNa-M4-1-c
SH-M4-2-c
SNa-M4-1-t
SH-M4-2-t
SNa-M4-1
SH-M4-2-A
SH-M4-2-B
SH-M4-1-Ba
SH-M4-1-Ac
Na-M4
5 6 7 8 9
2θ

Fig. 6

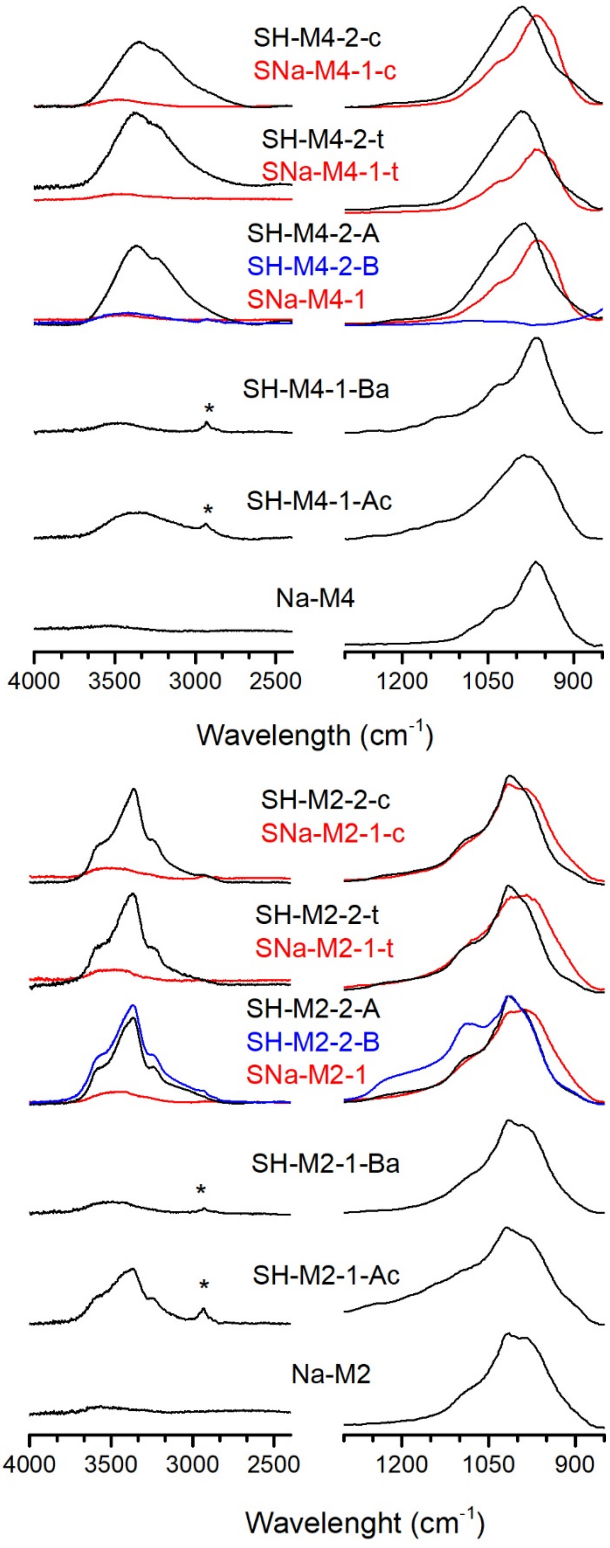
SH-M4-2-c
SNa-M4-1-c
SH-M4-2-t
SNa-M4-1-t
SH-M4-2-A
SH-M4-2-B
SNa-M4-1
SH-M4-1-Ba
SH-M4-1-Ac
Na-M4
4000
3500
3000
2500
1200
1050
900
Wavelength (cm-1)
SH-M2-2-c
SNa-M2-1-c
SH-M2-2-t
SNa-M2-1-t
SH-M2-2-A
SH-M2-2-B
SNa-M2-1
SH-M2-1-Ba
SH-M2-1-Ac
Na-M2
4000
3500
3000
2500
1200
1050
900
Wavelenght (cm-1)

Fig. 7

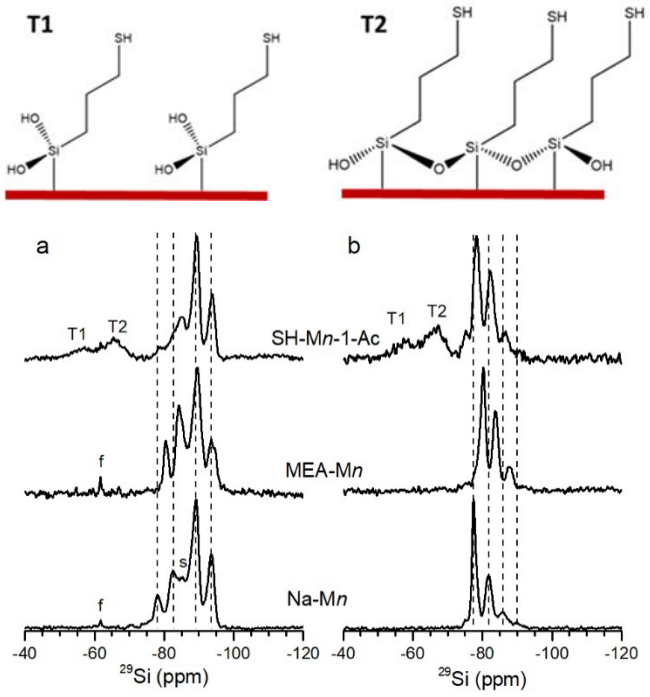
T1
T2
SH
HO
Si
O
OH
a
b
T1
T2
f
s
SH-Mn-1-Ac
MEA-Mn
Na-Mn
-40
-60
-80
-100
-120
29Si (ppm)

Fig. 8

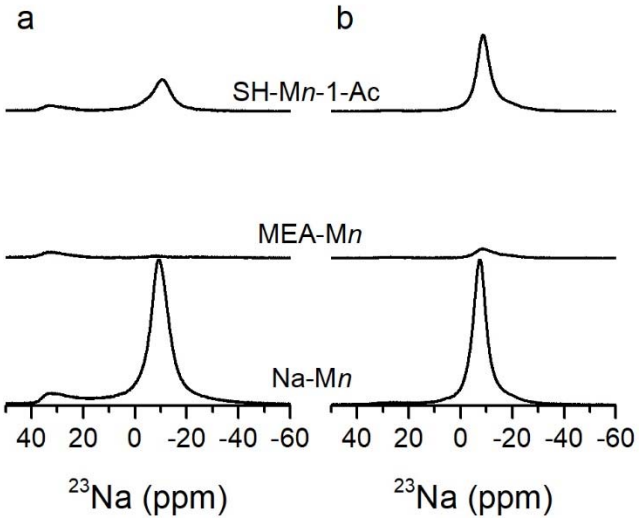
a
b
SH-Mn-1-Ac
MEA-Mn
Na-Mn
40 20 0 -20 -40 -60
40 20 0 -20 -40 -60
23Na (ppm)
23Na (ppm)

Fig. 9

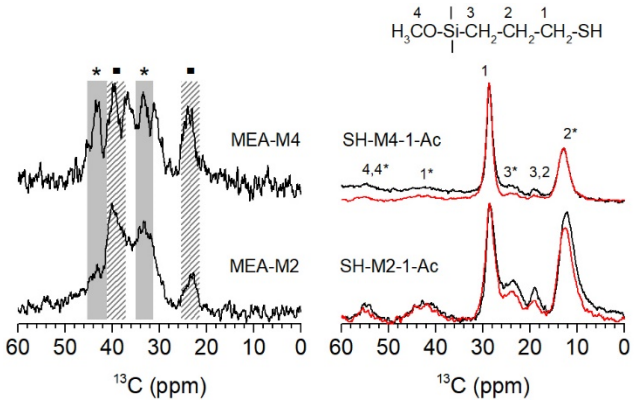
4 | 3 2 1
H3CO-Si-CH2-CH2-CH2-SH
|
MEA-M4
MEA-M2
SH-M4-1-Ac
SH-M2-1-Ac
4,4*
1*
3*
3,2
2*
60 50 40 30 20 10 0
13C (ppm)

Fig. 10

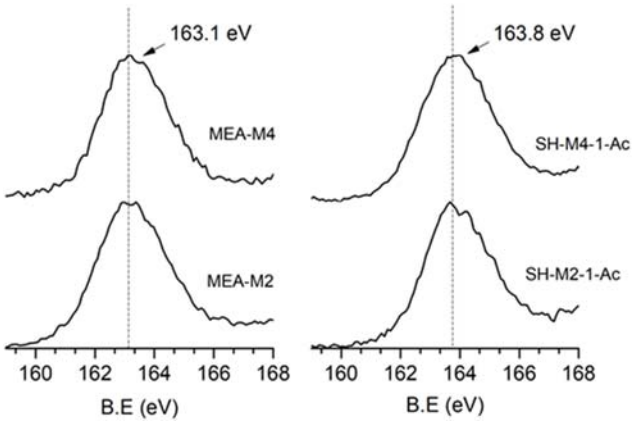
163.1 eV
MEA-M4
MEA-M2
160
162
164
166
168
B.E (eV)
163.8 eV
SH-M4-1-Ac
SH-M2-1-Ac
160
162
164
166
168
B.E (eV)

GRAPHICAL ABSTRACT

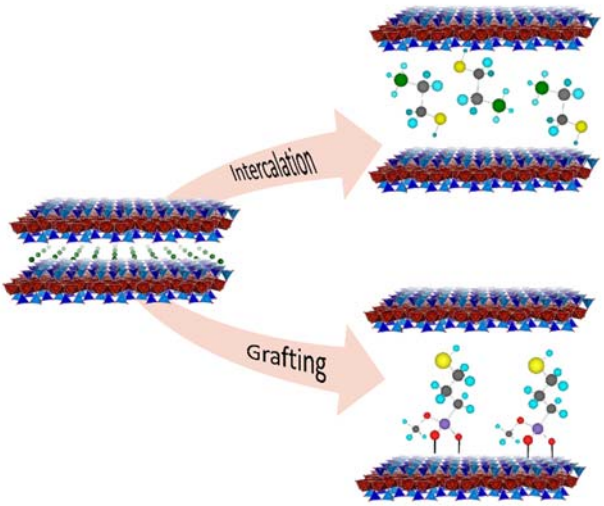

References

[1] A.G.N. Wamba, G.P. Kofa, S.N. Koungou, P.S. Thue, E.C. Lima, G.S. dos Reis, J.G. Kayem, Grafting of Amine functional group on silicate based material as adsorbent for water purification: A short review, Journal of Environmental Chemical Engineering 6(2) (2018) 3192-3203.

[2] G.P. Kofa, S. NdiKoungou, G.J. Kayem, R. Kamga, Adsorption of arsenic by natural pozzolan in a fixed bed: Determination of operating conditions and modeling, Journal of Water Process Engineering 6 (2015) 166-173.

[3] M. Anbia, S. Salehi, Removal of acid dyes from aqueous media by adsorption onto amino-functionalized nanoporous silica SBA-3, Dyes and Pigments 94(1) (2012) 1-9.

[4] S.M. Lee, D. Tiwari, Organo and inorgano-organo-modified clays in the remediation of aqueous solutions: An overview, Applied Clay Science 59-60 (2012) 84-102.

[5] V.E. dos Anjos, J.R. Rohwedder, S. Cadore, G. Abate, M.T. Grassi, Montmorillonite and vermiculite as solid phases for the preconcentration of trace elements in natural waters: Adsorption and desorption studies of As, Ba, Cu, Cd, Co, Cr, Mn, Ni, Pb, Sr, V, and Zn, Applied Clay Science 99 (2014) 289-296.

[6] M. Cruz-Guzman, R. Celis, M.C. Hermosin, W.C. Koskinen, E.A. Nater, J. Cornejo, Heavy metal adsorption by montmorillonites modified with natural organic cations, Soil Science Society of America Journal 70(1) (2006) 215-221.

[7] L. Mercier, T.J. Pinnavaia, A functionalized porous clay heterostructure for heavy metal ion (Hg2+) trapping, Microporous Mesoporous Mat. 20(1-3) (1998) 101-106.

[8] F. Wypych, Chemical modification of clay surfaces, Taylor and Francis, New York, 2006.

[9] J. Konya, N.M. Nagy, Sorption of dissolved mercury (II) species on calcium-montmorillonite: an unusual pH dependence of sorption process, Journal of Radioanalytical and Nuclear Chemistry 288(2) (2011) 447-454.

[10] Y. Cohen, V. Nguyen, J.D. Jou, N. Bei, W. Yoshida, Surface modification of inorganic oxide surfaces by graft polymerization, CRC Press, New York, 2001.

[11] L. Mercier, C. Detellier, Characterization and applications as heavy-metals sorbents of covalently grafted thiol functionalities on the interlamellar surface of montmorillonite, Environ. Sci. Technol. 29(5) (1995) 1318-1323.

[12] S.-J. Park, B.-J. Kim, D.-I. Seo, K.-Y. Rhee, Y.-Y. Lyu, Effects of a silane treatment on the mechanical interfacial properties of montmorillonite/epoxy nanocomposites, Materials Science and Engineering a-Structural Materials Properties Microstructure and Processing 526(1-2) (2009) 74-78.

[13] X.-Y. Zhang, Q.-C. Wang, S.-Q. Zhang, X.-J. Sun, Z.-S. Zhang, Stabilization/solidification (S/S) of mercury-contaminated hazardous wastes using thiol-functionalized zeolite and Portland cement, Journal of Hazardous Materials 168(2-3) (2009) 1575-1580.

[14] O. Gok, A.S. Ozcan, A. Ozcan, Adsorption behavior of a textile dye of Reactive Blue 19 from aqueous solutions onto modified bentonite, Applied Surface Science 256(17) (2010) 5439-5443.

[15] B. Sarkar, Y. Xi, M. Megharaj, R. Naidu, Orange II adsorption on palygorskites modified with alkyl trimethylammonium and dialkyl dimethylammonium bromide - An isothermal and kinetic study, Applied Clay Science 51(3) (2011) 370-374.

[16] Q. Tao, Y. Fang, T. Li, D. Zhang, M. Chen, S. Ji, H. He, S. Komarneni, H. Zhang, Y. Dong, Y.D. Noh, Silylation of saponite with 3-aminopropyltriethoxysilane, Applied Clay Science 132 (2016) 133-139.

[17] L. Su, T. Shu, Z. Wang, J. Cheng, F. Xue, C. Li, X. Zhang, Immobilization of bovine serum albumin-protected gold nanoclusters by using polyelectrolytes of opposite charges for the development of the reusable fluorescent Cu2+-sensor, Biosensors & Bioelectronics 44 (2013) 16-20.

[18] A. Saad, I. Bakas, J.-Y. Piquemal, S. Nowak, M. Abderrabba, M.M. Chehimi, Mesoporous silica/polyacrylamide composite: Preparation by UV-graft photopolymerization, characterization and use as Hg(II) adsorbent, Applied Surface Science 367 (2016) 181-189.

[19] W. Shan, Y. Shu, H. Chen, D. Zhang, W. Wang, H. Ru, Y. Xiong, The recovery of molybdenum(VI) from rhenium(VII) on amino-functionalized mesoporous materials, Hydrometallurgy 165 (2016) 251-260.

[20] C. Liu, P. Wu, T. Lytuong, N. Zhu, Z. Dang, Organo-montmorillonites for efficient and rapid water remediation: sequential and simultaneous adsorption of lead and bisphenol A, Environmental Chemistry 15(5) (2018) 286-295.

[21] M.D. Alba, M.A. Castro, M. Naranjo, E. Pavon, Hydrothermal reactivity of Na-n-micas (n=2, 3, 4), Chemistry of Materials 18(12) (2006) 2867-2872.

[22] Y. Morikawa, T. Goto, Y. Morooka, T. Ikawa, Conversion of methanol over metal-ion exchanged forms of fluor tetra silisic mica, Chemistry Letters (10) (1982) 1667-1670.

[23] W.J. Paulus, S. Komarneni, R. Roy, Bulk synthesis and selective exchange of strontium ions in Na4Mg6Al4Si4O20F4 mica, Nature 357(6379) (1992) 571-573.

[24] M. Gregorkiewitz, J.A. Rausellcolom, Characterization and properties of a new synthetic silicate with highly charged mica-type layers, Am. Miner. 72(5-6) (1987) 515-527.

[25] D. Malferrari, M.F. Brigatti, A. Laurora, S. Pini, L. Medici, Sorption kinetics and chemical forms of Cd(II) sorbed by thiol-functionalized 2 : 1 clay minerals, Journal of Hazardous Materials 143(1-2) (2007) 73-81.

[26] A.C.V. dos Santos, J.C. Masini, Evaluating, the removal of Cd(II), Pb(II) and Cu(II) from a wastewater sample of a coating industry by adsorption onto vermiculite, Applied Clay Science 37(1-2) (2007) 167-174.

[27] A.d.M. Ferreira Guimaraes, V.S.T. Ciminelli, W.L. Vasconcelos, Smectite organofunctionalized with thiol groups for adsorption of heavy metal ions, Applied Clay Science 42(3-4) (2009) 410-414.

[28] D.L. Guerra, M.R.M.C. Santos, C. Airoldi, Mercury Adsorption on Natural and Organofunctionalized Smectites - Thermodynamics of Cation Removal, J. Braz. Chem. Soc. 20(4) (2009) 594-603.

[29] M. Jaber, J. Miehe-Brendle, L. Michelin, L. Delmotte, Heavy metal retention by organoclays: Synthesis, applications, and retention mechanism, Chemistry of Materials 17(21) (2005) 5275-5281.

[30] R. Martin-Rodriguez, F. Aguado, M.D. Alba, R. Valiente, A.C. Perdigon, Eu3+ Luminescence in High Charge Mica: An In Situ Probe for the Encapsulation of Radioactive Waste in Geological Repositories, ACS Appl. Mater. Interfaces 11(7) (2019) 7559-7565.

[31] F.J. Osuna, A. Cota, E. Pavon, M.C. Pazos, M.D. Alba, Cesium adsorption isotherm on swelling high-charged micas from aqueous solutions: Effect of temperature, Am. Miner. 103(4) (2018) 623-628.

[32] F.J. Osuna, A. Cota, E. Pavon, M.C. Pazos, M.D. Alba, Cs+ immobilization by designed micaceous adsorbent under subcritical conditions, Applied Clay Science 143 (2017) 293-299.

[33] M.J. Garcia-Jimenez, A. Cota, F.J. Osuna, E. Pavon, M.D. Alba, Influence of temperature and time on the Eu3+ reaction with synthetic Na-Mica-n (n=2 and 4), Chemical Engineering Journal 284 (2016) 1174-1183.

[34] L. Tran, P.X. Wu, Y.J. Zhu, L. Yang, N.W. Zhu, Highly enhanced adsorption for the removal of Hg(II) from aqueous solution by Mercaptoethylamine/Mercaptopropyltrimethoxysilane functionalized vermiculites, Journal of Colloid and Interface Science 445 (2015) 348-356.

[35] L. Tran, P. Wu, Y. Zhu, S. Liu, N. Zhu, Comparative study of Hg(II) adsorption by thiol- and hydroxyl-containing bifunctional montmorillonite and vermiculite, Applied Surface Science 356 (2015) 91-101.

[36] R. Celis, M.C. Hermosin, J. Cornejo, Heavy metal adsorption by functionalized clays, Environ. Sci. Technol. 34(21) (2000) 4593-4599.

[37] A. Walcarius, M. Etienne, J. Bessiere, Rate of access to the binding sites in organically modified silicates. 1. Amorphous silica gels grafted with amine or thiol groups, Chemistry of Materials 14(6) (2002) 2757-2766.

[38] E. Pavon, M.A. Castro, M. Naranjo, M.M. Orta, M.C. Pazos, M.D. Alba, Hydration properties of synthetic high-charge micas saturated with different cations: An experimental approach, Am. Miner. 98(2-3) (2013) 394-400.

[39] M.D. Alba, M.A. Castro, M. Naranjo, M.M. Orta, E. Pavon, M.C. Pazos, Evolution of Phases and Al-Si Distribution during Na-4-Mica Synthesis, J. Phys. Chem. C 115(41) (2011) 20084-20090.

[40] J. Zhou, P. Wu, Z. Dang, N. Zhu, P. Li, J. Wu, X. Wang, Polymeric Fe/Zr pillared montmorillonite for the removal of Cr(VI) from aqueous solutions, Chemical Engineering Journal 162(3) (2010) 1035-1044.

[41] C.J. Liao, C.P. Chen, M.K. Wang, P.N. Chiang, C.W. Pai, Sorption of chlorophenoxy propionic acids by organoclay complexes, Environmental Toxicology 21(1) (2006) 71-79.

[42] P. Wu, Y. Dai, H. Long, N. Zhu, P. Jai, J. Wu, Z. Dang, Characterization of organo-montmorillonites and comparison for Sr(II) removal: Equilibrium and kinetic studies, Chemical Engineering Journal 191 (2012) 288-296.

[43] X. Yu, C. Wei, L. Ke, Y. Hu, X. Xie, H. Wu, Development of organovermiculite-based adsorbent for removing anionic dye from aqueous solution, Journal of Hazardous Materials 180(1-3) (2010) 499-507.

[44] K. Rajalakshmi, G. Kalaiarasi, Vibrational and Spectroscopic Analysis on 2,3-Dimercapto-1- Propanol by HF and DFT Calculations, International Journal of Current Research and Review 10 (2018) 94-98.

[45] G. Li, Z. Zhao, J. Liu, G. Jiang, Effective heavy metal removal from aqueous systems by thiol functionalized magnetic mesoporous silica, Journal of Hazardous Materials 192(1) (2011) 277-283.

[46] M.D. Alba, A.I. Becerro, M.A. Castro, A.C. Perdigon, Hydrothermal reactivity of Lu-saturated smectites: Part I. A long-range order study, Am. Miner. 86(1-2) (2001) 115-123.

[47] M.D. Alba, A.I. Becerro, M.A. Castro, A.C. Perdigon, Hydrothermal reactivity of Lu-saturated smectites: Part II. A short-range order study, Am. Miner. 86(1-2) (2001) 124-131.

[48] G.E. Christidis, P.W. Scott, A.C. Dunham, Acid activation and bleaching capacity of bentonites from the islands of Milos and Chios, Aegean, Greece, Applied Clay Science 12(4) (1997) 329-347.

[49] D.M. Moore, R.C. Reynolds, Oxford University Press, New York, 1997.

[50] Z. Vukovic, A. Milutonovic, L. Rozic, A. Rosic, Z. Nedic, D. Jovanovic, The influence of acid treatment on the composition of bentonite, Clay Clay Min. 54(6) (2006) 697-702.

[51] F.H. do Nascimento, D.M. de Souza Costa, J.C. Masini, Evaluation of thiol-modified vermiculite for removal of Hg(II) from aqueous solutions, Applied Clay Science 124 (2016) 227-235.

[52] J. Madejova, J. Bujdak, M. Janek, P. Komadel, Comparative FT-IR study of structural modifications during acid treatment of dioctahedral smectites and hectorite, Spectrochimica Acta Part a-Molecular and Biomolecular Spectroscopy 54(10) (1998) 1397-1406.

[53] M. Magi, E. Lippmaa, A. Samoson, G. Engelhardt, A.R. Grimmer, Solid-state high-resolution Si-29 chemical-shifts in silicates, Journal of Physical Chemistry 88(8) (1984) 1518-1522.

[54] E. Pavon, F.J. Osuna, M.D. Alba, L. Delevoye, Direct evidence of Lowenstein's rule violation in swelling high-charge micas, Chemical Communications 50(53) (2014) 6984-6986.

[55] E. Pavon, F.J. Osuna, M.D. Alba, L. Delevoye, Natural abundance O-17 MAS NMR and DFT simulations: New insights into the atomic structure of designed micas, Solid State Nucl. Magn. Reson. 100 (2019) 45-51.

[56] W.D. Johns, P.K. Sengupta, Vermiculite-alkyl ammonium complexes, Am. Miner. 52(11-1) (1967) 1706-&.

[57] G. Lagaly, Layer Charge Determination by Alkylammonium Ions, in Charge Characteristics of 2:1 Clay Minerals, the Chemistry of Clay-Organic Reactions, Clay Mineral Society, USA, 1994.

[58] J. Sanz, J.M. Serratosa, SI-29 and Al-27 high-resolution MAS-NMR spectra of phyllosilicates, J. Am. Chem. Soc. 106(17) (1984) 4790-4793.

[59] S. Komarneni, R. Pidugu, W. Hoffbauer, H. Schneider, A synthetic Na-rich mica: Synthesis and characterization by Al-27 and Si-29 magic angle spinning nuclear magnetic resonance spectroscopy, Clay Clay Min. 47(4) (1999) 410-416.

[60] S. Komarneni, R. Pidugu, J.E. Amonette, Synthesis of Na-4-mica from metakaolinite and MgO: characterization and Sr2+ uptake kinetics, J. Mater. Chem. 8(1) (1998) 205-208.

[61] V. Laperche, J.F. Lambert, R. Prost, J.J. Fripiat, High-resolution solid-state nmr of exchangeable cations in the interlayer surface of a swelling Miica - Na-23, Cd-111, and Cs-133 vermiculites, Journal of Physical Chemistry 94(25) (1990) 8821-8831.

[62] Z. Zeng, D. Matuschek, A. Studer, C. Schwickert, R. Poettgen, H. Eckert, Synthesis and characterization of inorganic-organic hybrid materials based on the intercalation of stable organic radicals into a fluoromica clay, Dalton Transactions 42(24) (2013) 8585-8596.

[63] PerkinElmer, ChemDraw Professional, 1998-2017.

[64] F.J. Osuna, A. Cota, M.A. Fernandez, E. Pavon, R.M. Torres Sanchez, M.D. Alba, Influence of framework and interlayer on the colloidal stability of design swelling high-charged micas, Colloids and Surfaces a-Physicochemical and Engineering Aspects 561 (2019) 32-38.

[65] M.G. da Fonseca, C. Airoldi, New layered inorganic-organic nanocomposites containing n-propylmercapto copper phyllosilicates, J. Mater. Chem. 10(6) (2000) 1457-1463.

[66] I.J. Dijs, H.L.F. van Ochten, C.A. van Walree, J.W. Geus, L.W. Jenneskens, Alkyl sulphonic acid surface-functionalised silica as heterogeneous acid catalyst in the solvent-

free liquid-phase addition of acetic acid to camphene, Journal of Molecular Catalysis a-Chemical 188(1-2) (2002) 209-224.

[67] C.A. Quirarte-Escalante, V. Soto, W. de la Cruz, G.R. Porras, R. Manriquez, S. Gomez-Salazar, Synthesis of Hybrid Adsorbents Combining Sol-Gel Processing and Molecular Imprinting Applied to Lead Removal from Aqueous Streams, Chemistry of Materials 21(8) (2009) 1439-1450.